Journal of Molecular Structure 1247 (2022) 131308

Contents lists available at ScienceDirect

Journal of Molecular Structure

journal homepage: www.elsevier.com/locate/molstr

Crystal structure, physicochemical, DFT, optical, keto-enol tautomerization, docking, and anti-diabetic studies of (*Z*)-pyrazol β-keto-enol derivative

Said Tighadouini[a,*], Othmane Roby[a], Salma Mortada[b], Zouhair Lakbaibi[c,d], Smaail Radi[e], Anas Al-Ali[f], My El Abbes Faouzi[b], Marilena Ferbinteanu[g], Yann Garcia[h], Nabil Al-Zaqri[i], Abdelkader Zarrouk[j], Ismail Warad[k,*]

[a] *Laboratory of Organic Synthesis, Extraction and Valorization, Faculty of Sciences Ain Chock, Hassan II University, Route d'El Jadida Km 2, Casablanca BP 5366, Morocco*
[b] *Laboratory of Pharmacology and Toxicology, Biopharmaceutical and toxicological analysis research team, Faculty of Medicine and Pharmacy, University Mohammed V of Rabat, Morocco*
[c] *Laboratory of Materials Engineering, Natural Resources and Environment (LMENRE), Department of Chemistry, Faculty of Sciences and Techniques Errachidia, My Ismail University, BP 509, Boutalamine, Errachidia, Morocco*
[d] *Laboratory of Molecular Chemistry, Materials and Environment (LCM2E), Multidisciplinary faculty Nador, Mohammed first University, B.P: 300 Selouane, Oujda, Nador 62700, Morocco*
[e] *Laboratory of Applied and Environmental Chemistry (LCAE), Mohammed first University, Oujda, Morocco*
[f] *Department of Chemistry, Science College, An-Najah National University, P.O. Box 7, Nablus, Palestine*
[g] *Faculty of Chemistry, Inorganic Chemistry Department, University of Bucharest, Bucharest 020462, Romania*
[h] *Molecular Chemistry, Materials and Catalysis Division (IMCN/MOST), Institute of Condensed Matter and Nanosciences, Université catholique de Louvain, Louvain-la-Neuve 1348, Belgium*
[i] *Department of Chemistry, College of Science, King Saud University, P.O. Box 2455, Riyadh 11451, Saudi Arabia*
[j] *Laboratory of Materials, Nanotechnology, and Environment, Faculty of Sciences, Mohammed V University in Rabat, P.O. Box. 1014, Agdal-Rabat, Morocco*
[k] *Department of Chemistry and Earth Sciences, PO Box 2713, Qatar University, Doha, Qatar*

ARTICLE INFO

Article history:
Received 9 February 2021
Revised 1 August 2021
Accepted 13 August 2021
Available online 17 August 2021

Keywords:
β-keto-enol
α-glucosidase
Docking
DFT
Thermal
XRD

ABSTRACT

The new (*Z*)-pyrazol β-keto-enol as model-molecule has been prepared in accepted high yield; the structure was investigated by X-ray single crystal diffraction (XRD) and Density Functional Theory (DFT) modeling. Several hydrogen bonds interactions were recorded experimentally *via* XRD and theoretically *via* Hirshfeld surface analysis (HSA) calculations. The recorded vibrational frequencies FT-IR were further compared to computed ones. Natural Population Analysis (NPA), Mulliken Atomic Charge (MAC), and Molecular Electrostatic Potential (MEP) has been carried out to complete the set of theoretical tools. The HOMO/LUMO, density of state (DOS) and TD-SCF/DFT were applied to compare these quantum parameters with experimental electron transfer and direct optical activity. DFT calculations, natural bond orbital (NBO) analysis and non-covalent interactions (NCI) analysis were used to explore the mechanism of the single proton keto-enol intra-migration tautomerization reaction. Additionally, the desired compound was screened for its *in-vitro* α-amylase and α-glucosidase inhibitory activities. The title compound reflected a potent inhibitory activity α-glucosidase enzyme with IC_{50} value of 72.20 ± 1.50 µM. Moreover, the solved 3D-crystal structure was used for 1BNA DNA docking evaluation.

1. Introduction

β-ketoenols compounds are interesting in pharmaceutical and medical fields, and are used as drugs against cancer, HIV, influenza, anti-inflammatory and antioxidant substances [1–8]. Derivatives of the β-keto-enol were used as chelate O∩O ligands that play a good turn in developing the coordination and complexation chemistry, since such compounds can stabilize several transition metals complexes *via* their polydentate mode of coordination [9–11].

The ketoenol associated with a pyrazole unit revealed molecules with combination properties; the chelate effect is supported furthermore *via* nitrogen atoms in the pyrazole part, which raised up the poly-chelate properties of the ligand that allowed the development of cluster coordination science [10–12].

* Corresponding authors.
E-mail addresses: tighadouinis@gmail.com (S. Tighadouini), ismail.warad@qu.edu.qa (I. Warad).

https://doi.org/10.1016/j.molstruc.2021.131308
0022-2860/

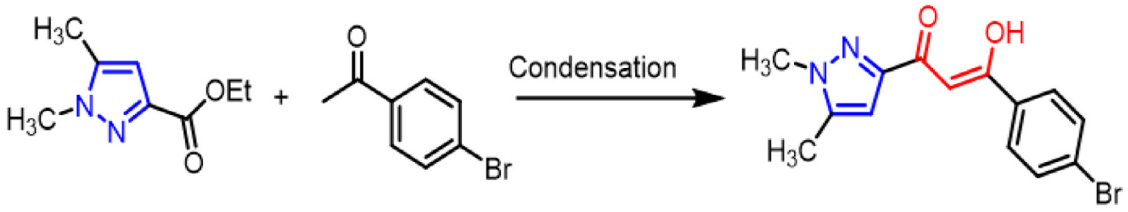

Scheme 1. Synthetic route for the desired (*Z*)-pyrazol β-keto-enol compound.

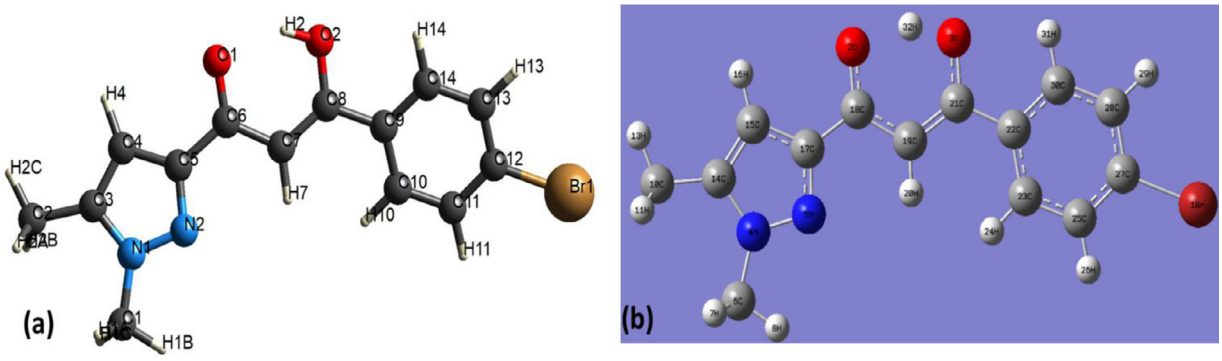

Fig. 1. (a) ORTEP, and (b) B3LYP/6-311++G(d,p) structures.

One of the simplest process and most significant one that have recently raised an immense interest is the intramolecular proton transfer (IPT). Most of the possible IPT phenomena have been found in keto–enol molecules having intra proton acceptors (C=O, C=N) and intra proton donors (N-H, O-H) modes *via* authentic synthon of type *n* [S(n)] intramolecular hydrogen bonds tautomerisms [13].

Keto–enol tautomerism services a decisive turn in molecules holding carbonyl functional group. Requesting the carbonyl tautomeric in molecules are significant to substantiate their critical biological applications and to comprehend biochemical reactions [14–19]. The best-known examples of tautomerism in organic materials with keto–enol functional groups are nitrogenous bases, which preserve the DNA double-strand structure *via* protons transfer to form new hydrogen bonds from the keto isomer. Keto-enol tautomerism of proton in hydroxyl group to its neighbor carbonyl functional group via single or double protons intra-migration have been investigated by means of experimental and theoretical methods [11–18]. However, several experimental and theoretical studies condoned the function of tautomeric process; nature of the proton movements (intra- or inter-molecular migration), accelerating or depressing factors, general mechanism and the role of H-bonding in stabilized both Keto and enol isomers structures [12–19].

In this work, we synthesized a new (*Z*)-pyrazol β-keto-enol compound which was subjected to XRD-analysis, HSA, spectral and several DFT-quantum, docking evaluation and DFT of the single proton keto-enol intra-migration tautomerization process. Moreover, the compound was screened for their *in-vitro* α-glucosidase and α-amylase inhibitory activities.

2. Experimental section

2.1. Computations and XRD

The DFT-calculations were performed at DFT/B3LYP/6-311++G(d,p) in gaseous phase via Gaussian09 program [20]. CRYSTAL EXPLORER 3.1 software was employed for HSA calculation [21]. The XRD-structure was employed using *SHELXS* program, respectively [22]. (Table S1 Supplementary Material)

2.2. BNA docking

Docking calculations were carried out at Intel(R) Core(TM) i7 CPU (3 GHz) with Windows 2010 software. The structure was drawn by ChemDraw. The docking was performed by assigning Gastegier charges. Water molecules were erased, and merging of non-polar hydrogen atoms was done using AutoDock.4 [23]. The X-ray crystal of PDB ID: 1BNA DNA was collected free from the Protein Data Bank [24].

2.2.1. Synthesis of (Z)-3-(4-Bromophenyl)-1-(1,5-dimethyl-1H-pyrazol-3-yl)-3-hydroxyprop-2-en-1-one

The β-keto–enol pyrazole derivative studied in this paper was prepared according to the experimental procedure described in our previous work [25]. 7.6 mmol of sodium metal was suspended in 30 mL of toluene before it was traded with 6.0 mmol of pyrazolic carboxylate dissolved also in 20 mL of toluene. Under 0 °C, 6.0 mmol of 3-bromophenyl methyl ketone 10 mL in toluene was added. The reaction mixture was stirred for 3 days at ambient air and room temperature. A precipitate was filtered, then cleaned well using aqueous acetic acid to pH = 5. The extracted organic product using CH_2Cl_2 was left to evaporate at room temperature. Yield ~ 40%.

Brown powder; yield: 32%; m.p 150 °C; R_f = 0.93 ($_{CH2Cl2}$/MeOh 9/1)/silica. IR (KBr, cm^{-1}): ν(OH)=3500-3300; ν(C=O) = 1670; ν (enolic C=C)=1565; ^{1}H NMR ($CDCl_3$): δ 2.30 (s, 3H, Pz-CH_3); 3.63 (s,3H, CH_3–N): 3.76 (s, 0.1H, keto, CH_2); 6.52 (s, 1H, pz–H); 6.69 (s, 0.9H, C–H); 7.72 (m, 2H, Ar–$H_{3.5}$); 7.85 (m, 2H, Ar–$H_{2.6}$). ^{13}C NMR ($CDCl_3$): δ 11.38 (1C, Pz-CH_3); 37.04 (1C, CH_3–N); 48.78 (1C, keto CH_2); 94.56 (1C, enol C–H); 106.45 (1C, -CH-pz); 121.94 (1C, Ar–C_4); 126.09 (2C, Ar–$C_{3.5}$); 129.22(2C, Ar–$C_{2.6}$); 180.54 (1C, C–OH); 183.59 (1C, C=O). Anal. Calcd. for $C_{14}H_{13}BrN_2O_2$: C 52.36, H 4.08, N 8.72. Found C 52.27, H 4.03, N 8.8; *m/z*: 321 $(M+H)^+$.

2.3. Antidiabetic activity

2.3.1. α-Glucosidase inhibition assay

The α-glucosidase inhibitory activity was performed in PBS (0.1M; pH 6.7), using ρ-nitrophenyl-α-D-glucopyranoside (ρNPG) as a substrate, following the method described by Lakbaibi et al.

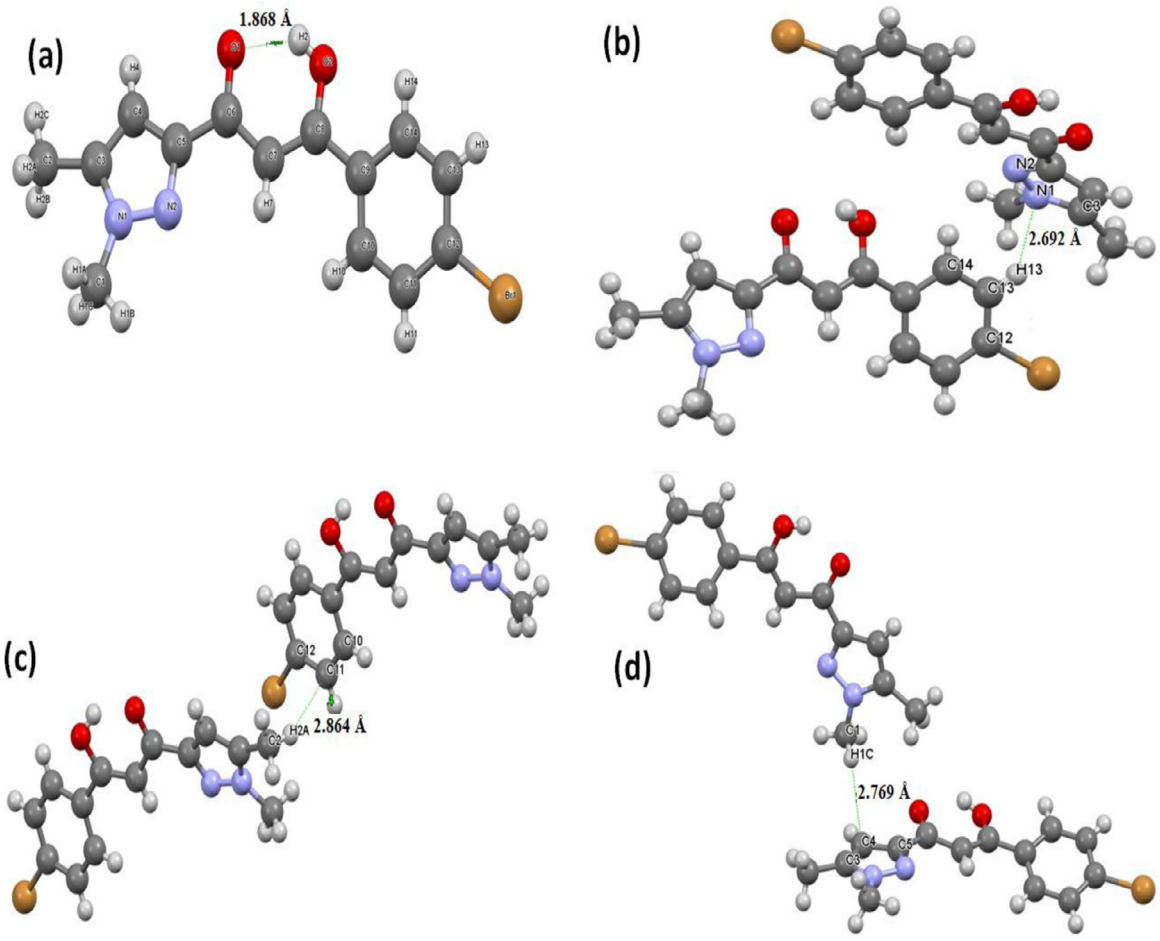

Fig. 2. H-bonds types and bond lengths.

[26], with some slight modifications. The samples were prepared by dissolving the title compound in DMSO and diluted in PBS to a series of different concentrations. Briefly, a mixture of 150 µL of the test sample and 100 µL of PBS containing the Baker's yeast *α-Glucosidase* enzyme solution (0.1 U/mL) were incubated at 37 °C for 10 min. Then, 200 µL of *ρ*NPG (1 mM) was added to the mixture to initiate the reaction. After incubation at 37 °C for 30 min, 1 mL Na_2CO_3 (0.1 M) was added to stop the reaction and the absorbance was measured at $\lambda = 405$ nm. The results were expressed as percentage inhibition and calculated using the following formula:

$$\text{Inhibition } (\%) = \left[\left(1 - \left(A_{\text{sample}} - A_{\text{b sample}}\right)\right)/\left(A_{\text{control}} - A_{\text{b control}}\right)\right] \times 100$$

Where A_{control} refers to the absorbance of the control (enzyme and buffer); $A_{\text{b control}}$ refers to the absorbance of control blank (buffer without enzyme); A_{sample} refers to the absorbance of the sample (enzyme and inhibitor); and $A_{\text{b sample}}$ is the absorbance of sample blank (inhibitor without enzyme). Acarbose was used as positive control.

2.3.2. α-amylase inhibition assay

The α-amylase inhibitory assay was performed by the protocol of Lakbaibi et al. [26] with some modifications. At first, the substrate was prepared by dissolving 200 mg starch in 25 mL of sodium hydroxide (0.4 M) with heating at 80 °C for 5 min. After cooling, pH was adjusted to 7.0 ± 0.1 and the final volume was completed to 100 mL with distilled water. Samples solution at varying concentrations (150 µL) were mixed with 500 µL of 0.02 M PBS (pH 6.9, 0.006M NaCl) containing the Human Pancreatic α-amylase enzyme (1.5 U/mL) and incubated for 10 min at 37 °C. Soluble starch (0.2%, PBS 0.02M, pH 6.9, 0.006M NaCl) was added to the mixture and further incubated at 37 °C for 10 min. The reaction was stopped by adding 250 µL of HCl (1M), followed by the addition of 300 µL of iodine reagent (5 mM), and the absorbance was measured at $\lambda = 630$ nm. The α-amylase inhibitory activity was expressed as percentage inhibition, and the IC_{50} values were determined. Acarbose was used as positive control.

3. Result and discussion

3.1. Synthesis CHN-EA and MS

The (Z)-pyrazol *β*-keto-enol compound was prepared in high yield *via* condensation of ethyl 1,5-dimethyl-1H-pyrazole-3-carboxylate with 2-(4-bromophenyl)-2-oxoethan-1-ylium at room temperature stirring for 48 h [20–25], as seen in Scheme 1.

Mass spectrometry of the desired compound was found to be 320.02 (theoretical 321.02), and the CHN-elemental analysis was found to be C, 52.42; H, 4.10 and N, 8.84, compared to the calculated from the general formula $C_{14}H_{13}BrN_2O_2$ to be C, 52.36; H, 4.08 and N, 8.72%.

3.2. XRD and DFT-structure analysis

The desired *β*-keto-enol crystallized in Z-kinetic favored isomer form with monoclinic, *P*21/n space-group, with four molecules in the unit-cell ($Z = 4$), as illustrated in Fig. 1a. The compound was stabilized in planar structure with very short intra-hydrogen bond

Table 1
DFT-calculated angles (°) and bond lengths (Å) compared to experimental XRD data.

Bond No.	Bonds		Exp. XRD	DFT	Angles No.	Angles (°)			Exp. XRD	DFT
1	Br1	C12	1.905	1.9282	1	N2	N1	C1	119	119.3
2	O1	C6	1.264	1.2888	2	N2	N1	C3	112.9	112.25
3	O2	C8	1.327	1.3442	3	C1	N1	C3	128	128.45
4	N1	N2	1.359	1.3907	4	N1	N2	C5	104.1	103.65
5	N1	C1	1.455	1.464	5	N1	C3	C2	123.2	122.82
6	N1	C3	1.364	1.3829	6	N1	C3	C4	106	106.21
7	N2	C5	1.337	1.352	7	C2	C3	C4	130.7	130.97
8	C2	C3	1.500	1.4972	8	C3	C4	C5	105.6	105.88
9	C3	C4	1.372	1.3822	9	N2	C5	C4	111.4	112.01
10	C4	C5	1.412	1.4165	10	N2	C5	C6	121.8	122.35
11	C5	C6	1.465	1.4591	11	C4	C5	C6	126.7	125.64
12	C6	C7	1.429	1.4251	12	O1	C6	C5	117.8	118.47
13	C7	C8	1.376	1.3792	13	O1	C6	C7	121.5	122.15
14	C8	C9	1.464	1.4746	14	C5	C6	C7	120.7	119.38
15	C9	C10	1.402	1.4032	15	C6	C7	C8	120.9	118.96
16	C9	C14	1.400	1.4035	16	O2	C8	C7	120.9	120.74
17	C10	C11	1.380	1.3916	17	O2	C8	C9	114.2	114.83
18	C11	C12	1.393	1.3914	18	C7	C8	C9	124.9	124.43
19	C12	C13	1.368	1.3903	19	C8	C9	C10	121.9	122.81
20	C13	C14	1.383	1.3911	20	C8	C9	C14	119.4	118.3

of type O-H…O=C [25–28]. In the gaseous phase, the B3LYP/6-311++G(d,p) optimized structure reflected also the presence of intra-hydrogen bond which is consistent with XRD-exp. result as seen in Table 1 and Fig. 1b.

DFT/XRD angles and bonds lengths values are in an excellent agreement (Table 1 and Fig. S1 of Supporting Materials), Bond length DFT and experimental values it was seen in Fig. S1, where the graphical correlation was found to be 0.9931 as in Fig. S1 b. closely, the graphical correlation between the DFT/XRD angles found to be 0.9844 (Fig. S1 c and d). The DFT parameters are slightly longer than the XRD ones since they are performed in the gaseous state, whereas the XRD was carried out in the solid-state.

3.3. Crystal interactions and HSA investigation

Two main H-bonds of types H….O and H…N were recorded in the lattice of the crystal [27–30], each molecule is binding with its surrounding *via* four total interactions (Fig. 2). Two H-bonds and two H…π interactions. The shortest interaction is in the β-keto-enol part since the proton of enol binds to the carbonyl oxygen of the keto part as O-H…O=C with 1.868 Å to form a S6 intra-synthon (Fig. 2a). An inter hydrogen bond of type C_{ph}-H….$N_{pyrazole}$ with 2.692 Å, forming a 1D supramolecular system was observed (Fig. 2b). The other H…π bonds were detected as C_{Me}-H…. π_{ph} 2.864 Å (Fig. 2c) and C_{Me}-H…. $\pi_{pyrazole}$ 2.769 Å (Fig. 2d).

In HSA, four red dots on the d_{norm} surface of the ligand molecule were detected [28–32]; all the d_{norm} big dots are due to the intra H…O and inter H….N hydrogen bonds formation (Fig. 3a). The shape index Fig. 4b reflected clearly the formation of H…π_{ring} bonds interactions. The number and the type of the H-bonds detected by HSA were matching with XRD-result interactions result (Fig. 3b). The HSA 2D-FP result plots over the ligand surface molecule revealed the presence of 58.5% H…overall connections. Atom-to-atom inter-contacts ratios are depicted in Fig. 3c with five types of H…interactions as: H…H (35.6%)> H…C (9.2%)> H…O (5.7%) > H…Br (4.9%) > H…N (4.9%).

3.4. MEP and atomic charge populations

The MEP suggested the presence of electrophilic/nucleophilic sites in the molecule surface as seen in Fig. 4a and b. For instance, the red color reflected hydroxyl oxygen, carbonyl O and pyrazole N atoms as the strongest nucleophile site. The Br atom with green color indicating that it is between electrophilic and nucleophilic centers. The blue colors of methyl and phenyl protons atoms reflected the electrophilic positions, except the proton atom of the hydroxide which is in green color since this atom is busy with intra-hydrogen bond, therefore it is not highlighted with blue color. Since both blue and red colors were detected via MEP, therefore several H-bonds were predictable [27,28]. These results matched well the XRD and HAS results.

MAC and NPA charges population revealed digital e-poor or e-rich molecule atoms as in Fig. 4c. Generally, MAC reflected less atomic-charges values compared to NPA. The MAC and NPA proved all the N and O atoms and (C6, C10, C15, C19, C20, C22, C23, C27, C28 and C30) atoms are with negative e-values (nucleophilic sites). The electrophilic sites are C14 and C21 atoms and all hydrogen atoms since they are with positive e values, therefore its electrophilic sites (see Table 2). Moreover, the NPA and MAC charges results are fitted well with the MEP, XRD and HSA results.

3.5. IR investigations

The solid state Exp.-IR and the DFT gaseous state of the desired ligand showed the presence of couple of functional groups in the backbone of the ligand. The O-H bond was not detected in both states with its expected frequencies at 3500–3300 cm^{-1} that supported the presence of intra hydrogen bond [25]. C-H_{ph} stretching vibrations were found at ~ 3110 cm^{-1}, C-H_{CH3} stretching vibrations at 2950–2840 cm^{-1} and C=O stretching vibrations at 1670 cm^{-1} as seen in Fig. 5a. Moreover, a high degree of correlation between the DFT-IR and Experiment was observed (Fig. 5b). This high degree of compatibility can be translated *via* 0.9927 graphical correlation values as seen in Fig. 5c.

3.6. HOMO-LUMO, DOS, optical and TD-DFT/e-transfer

HOMO/LUMO shapes and energy diagram (Fig. 6a) and DOS (Fig. 6b) showed the e-donation ability in the UV area with $\Delta E_{HOMO/LUMO}$ = 4.2327 and 4.2520 eV, respectively.

Experimentally, Tauc relation [33] can be used to check the energy matching between DOS and HOMO/LUMO theoretical result with optical band gap energy (ΔE_g) using DMSO solvent yielding to ΔE_g = 4.22 eV (Fig. 6c). The result is approximated to both $\Delta E_{HOMO/LUMO}$ and ΔE_{DOS} energy.

The experimental electron transfer and computed TD-DFT/B3LYP/6-311++G(d,p) in DMSO solvents was illustrated in Fig. 6d. Experimentally, two broad bands at λ_{max} = 230 and

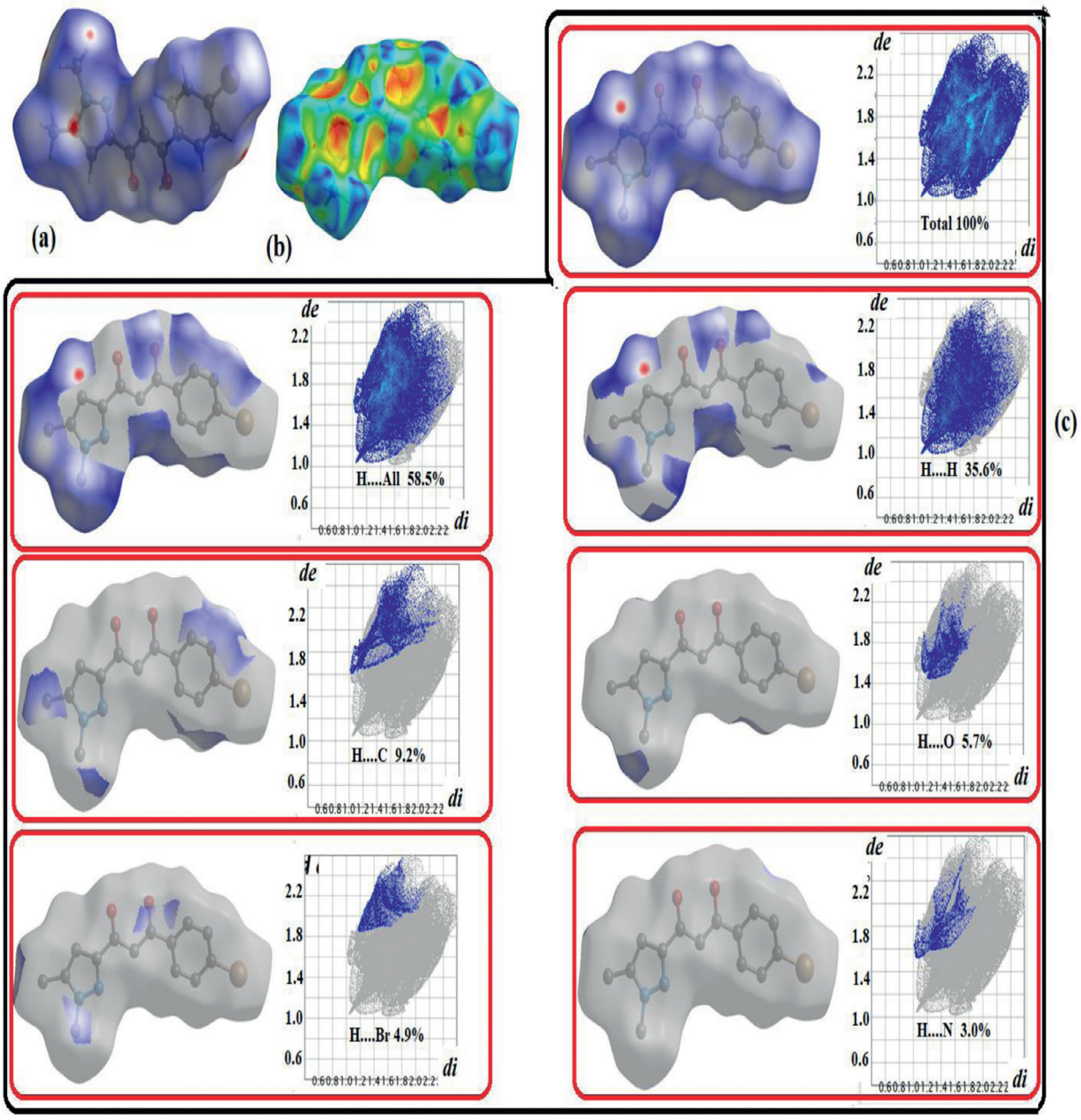

Fig. 3. (a) d_{norm} mapped (b) shape index, and (c) Fingerprint inside…outside atoms.

Table 2
Mac and NPA charge population.

Atoms No.	Atom type	MAC	NPA	Atoms No.	Atom type	MAC	NPA
1	Br	0.206289	0.11132	17	C	0.290033	0.08653
2	O	-0.49037	-0.48656	18	C	0.396422	0.43962
3	O	-0.58526	-0.64112	19	C	-0.28694	-0.36893
4	N	-0.3949	-0.24405	20	H	0.214996	0.24463
5	N	-0.37777	-0.24946	21	C	0.308859	0.34069
6	C	-0.40481	-0.46671	22	C	-0.02027	-0.10469
7	H	0.218281	0.23159	23	C	-0.1937	-0.20566
8	H	0.23553	0.24695	24	H	0.213562	0.2449
9	H	0.218747	0.22675	25	C	-0.14534	-0.22184
10	C	-0.62864	-0.70448	26	H	0.212826	0.25359
11	H	0.219565	0.2462	27	C	-0.34902	-0.1623
12	H	0.22655	0.24964	28	C	-0.14271	-0.24011
13	H	0.229027	0.25655	29	H	0.213245	0.25463
14	C	0.264418	0.14908	30	C	-0.18116	-0.19156
15	C	-0.27179	-0.30214	31	H	0.219605	0.2597
16	H	0.198791	0.25947	32	H	0.385917	0.48778

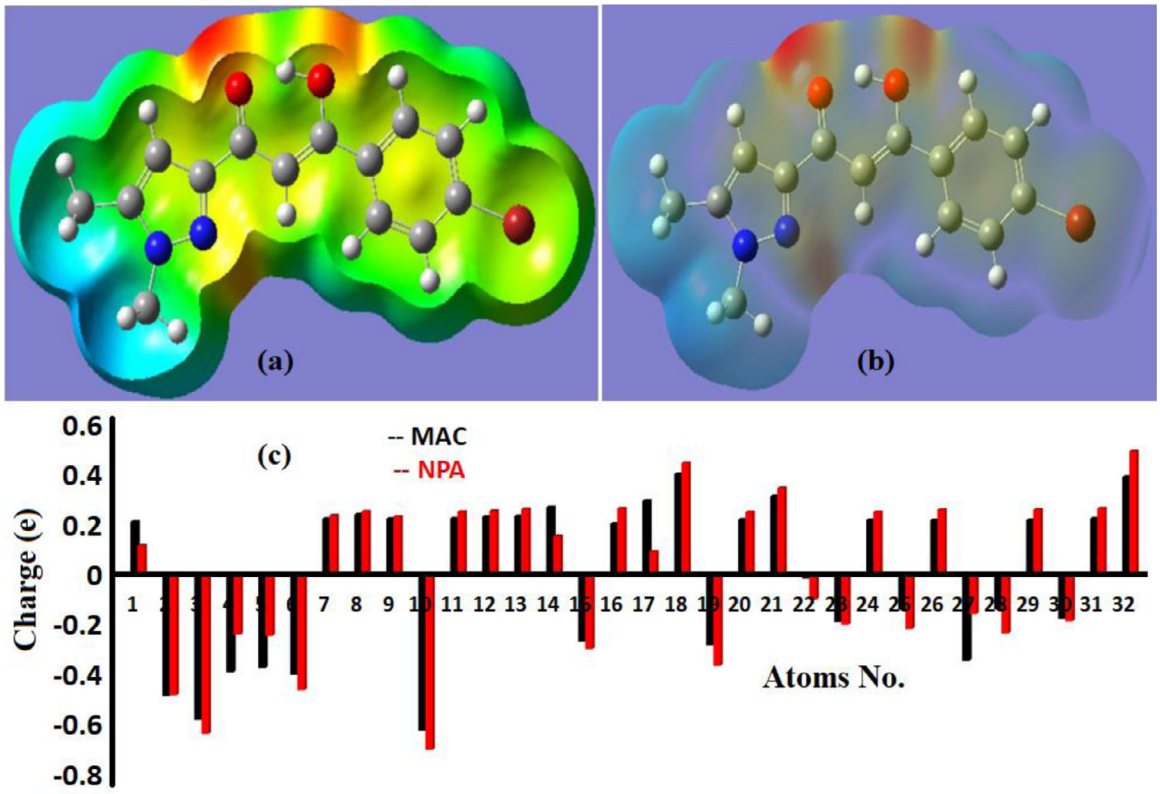

Fig. 4. (5) B3LYP/MEP, (a) libeled map and (b) BPA (■) and MAC (■) charge populations.

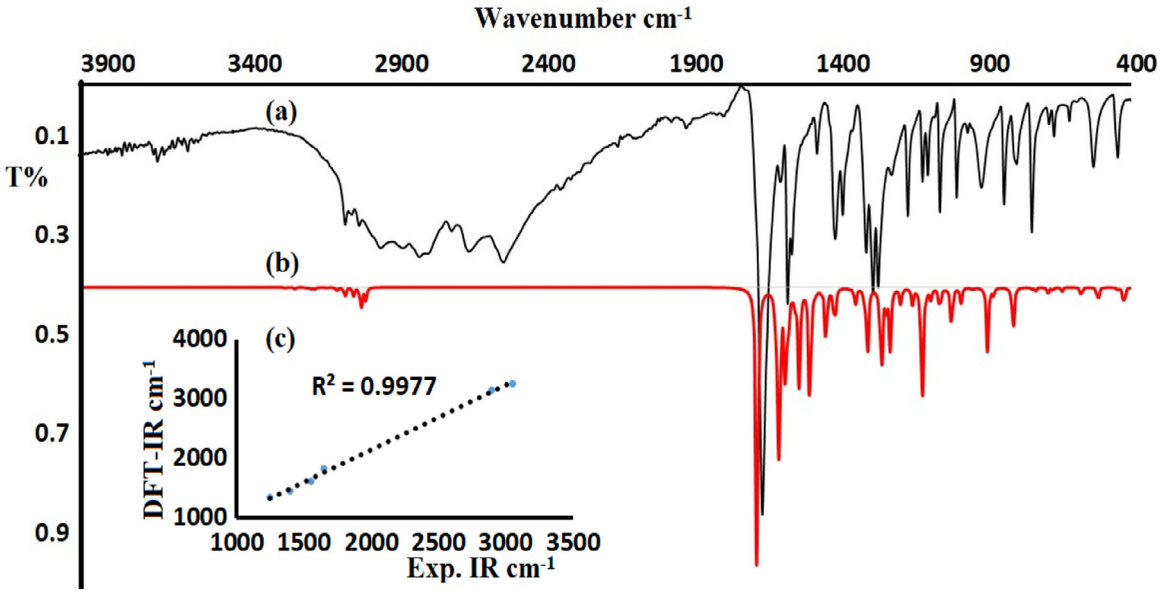

Fig. 5. IR of desired ligand (a) Exp. solid state (b) gaseous state DFT and (c) Exp./DFT graphical correlation.

λ_{max} = 312 nm corresponding mainly to $\pi \rightarrow \pi^*$ and $n \rightarrow \pi^*$ e-transition, were observed. No more bands were detected in the visible area. TD-DFT reflected a similar absorption behavior (Fig. 6d), two peaks with λ_{max} = 236 and λ_{max} = 315 nm were reported in DMSO, which is meanly assigned to HOMO-1 > LUMO+1 (12%), HOMO > LUMO+1 (18%), HOMO > LUMO+2 (50%) HOMO-5 > LUMO (7%), HOMO-5 > LUMO+1 (4%) and HOMO-4 > LUMO (4%) for peak at λ_{max}= 236 nm. Peak at λ_{max}= 315 nm is assigned to HOMO-1 > LUMO (11%), HOMO > LUMO (83%) and HOMO-3 > LUMO (2%). The small $\Delta\lambda$ shift between the Exp. and DFT peaks can be attributed to solvent-solute interaction [27–32].

3.7. Tautomerisation of diketone (DFT study)

3.7.1. Energetic profile of reaction

The transformation of diketone structure through tautomerisation process to (Z)-keto enol, (Z)-enol keto and (E)-enol keto was discussed (Fig. 7) under implicit SMD solvation of toluene, room temperature and 1 atm. All concerned structures out carried basing on DFT computations by applying the B3LYP exchange-correlation

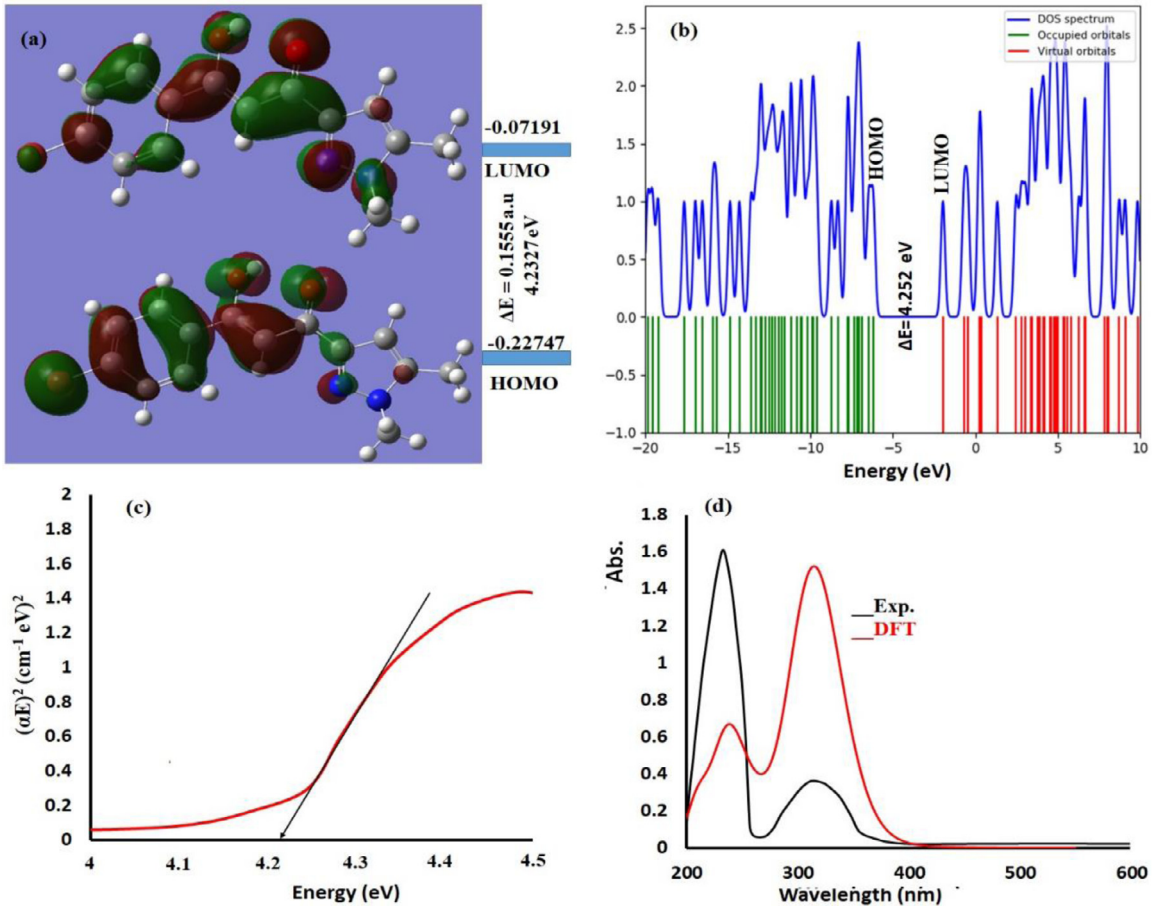

Fig. 6. (a) LUMO/HOMO, (b) TD-DFT, (c) Exp. electronic spectra, and (d) optical band gap energy in DMSO.

functional with 6–311G++(d,p) basis set [25,26]. Therefore, in order to contribute to a better understanding of the mechanism for this reaction and explain the most favorable tautomerization, we realized the various points as follows: a complete analysis of the Gibbs free energy difference profile of the reaction. Yet, a characterization of the transition-state TSs (i.e., TS-(Z)-keto enol and TS-(Z)-enol keto) associated with the tautomerism reaction was made using QST3 approach [34,35] (Fig. 8). All calculations were made at level NBO analysis [36].

According to the Fig. 8, the (Z)-keto enol is slightly more stable than (Z)-enol keto with 2.250 kcal/mol. The diketone tautomerization to both (Z)-keto enol and (Z)-enol keto has almost a similar aspect at level kinetic behavior. Therefore, we have noticed that the formation of (Z)-keto enol is slightly more favored than of (Z)-enol keto. Otherwise, it is noticed that the activation Gibbs free energy barrier corresponding to the formation of (Z)-keto enol is 44.238 kcal/mol, and for the formation of (Z)-enol keto is 46.114 kcal/mol; indicates clearly that the kinetic of formation of (Z)-keto enol is almost the same with (Z)-enol keto. This result indicates that both (Z)-keto enol and (Z)-enol keto products have the potential to form with a small dominance of (Z)-keto enol. As for the formation of (E)-enol keto its formation is difficult from diketone tautomerization (it is not possible).

3.7.2. NCI analysis

NCI analysis was also carried out on the three following possible structures (Z)-keto enol, (Z)-enol keto and (E)-enol keto which formed according to the studied reaction. NCIs analysis evaluates the intermolecular interactions and can be revealed solely by means of the reduced density gradient, S, which is a scalar field of the electron density (ρ) and can be defined as:

$$S = \frac{|\nabla\rho|}{2(3\pi^2)\rho^{4/3}}$$

The S function has higher values in regions outside the molecule and lower values near the covalent bonds and non-covalent interactions, which appear as peaks in the S(r) diagram [38]. The limiting interaction cases like hydrogen bonds, Van der Waals (VdW) and steric repulsion is reflected here with a coloring scheme (blue, green, and red, respectively). Lu and Chen [39] conducted the non-covalent interactions and their visualization was done with Visual Molecular Dynamics VMD [40].

In other words, we observed from NCI analysis (Fig. 9) that both (Z)-keto enol and (Z)-enol keto present a hydrogen bond interaction between Hα and O1 which considered as strong interaction (32.15 and 26.04 kcal/mol, respectively, calculated from NBO analysis), much higher than the usual hydrogen bonds energies of 4–6 kcal/mol [41]. Additionally, as for (E)-enol keto we have remarked that there are existence of repulsive interactions between two hydrogen atoms (H6 & H7) and between oxygen and nitrogen atoms (O5 & N6). It is worth mentioning here that the strong hydrogen bond at the (Z)-keto enol and (Z)-enol keto favor their formation with respect to that of (E)-enol keto (presence of repulsive interactions).

3.8. Anti-diabetic activity

The antidiabetic activity of the title compound has been systematically evaluated against α-glucosidase and α-amylase at different concentration. The IC_{50} values of the *in-vitro* α-glucosidase

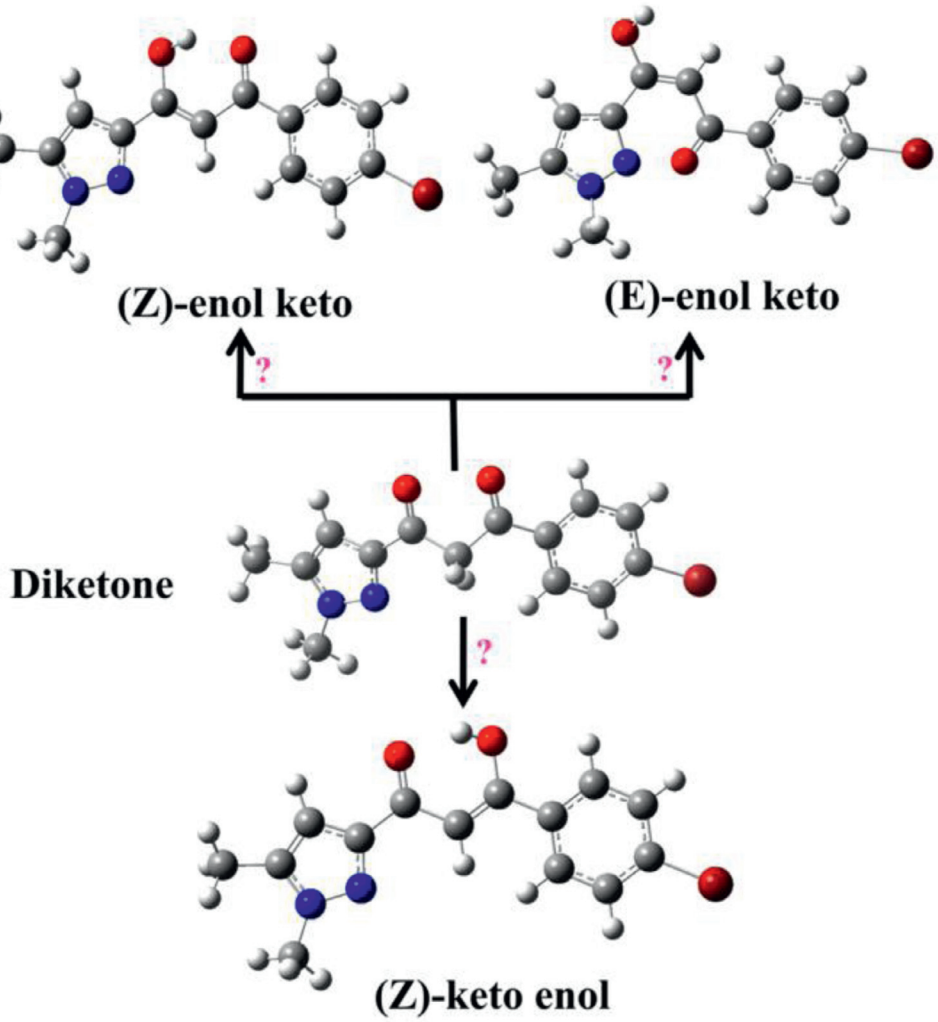

Fig. 7. Possible structures from diketone tautomerisation.

Table 3
Antidiabetic activity of (*Z*)-pyrazol β-keto-enol

Compound	IC_{50} (µM)[a]	
	α-glucosidase	α-amylase
(*Z*)-pyrazol β-keto-enol	72.20 ± 1.50	211.10 ± 1.06
Acarbose	72.58 ± 1.39	101 ± 1.95

[a] The IC_{50} values are mean ± SEM of three independent experiments.

and α-amylase inhibitory activities of the title molecule, compared to acarbose as reference drug are shown in Table 3. *In-vitro* study on the inhibition of α-glucosidase shows that the (*Z*)-pyrazol β-keto-enol has potent activity with IC_{50} value of 72.20 ± 1.50 µM, compared to acarbose (IC_{50} = 72.58 ± 1.39 µM). The results of the *in-vitro* α-amylase inhibitory activity reveal that (*Z*)-pyrazol β-keto-enol has a good inhibitory activity with IC_{50} value of 211.10 ± 1.06 µM. This value is 2.09-fold lower than that of acarbose (IC_{50} = 101 ± 1.95 µM) (Table 3).

3.9. Molecular docking

The solved XRD-structure of the desired ligand was docked to the DNA (PDB ID: 1BNA) available data [41], compound was cross-linked to both two DNA helix *via* four basic hydrogen bonds to form the [DNA:ligand] complex similar to *cis*-plat mode of binding (Fig. 10a). One of two Me functional group contributed to non-sufficient DNA binding *via* very long H-bonds 3.76 Å, since it is not impeded well in between the DNA helix, which supported the minor groove DNA intercalation. The docking effect can be considered as good data when the Root Mean Square Deviation (RMSD) value is less than 2 Å [32]. The other three H-bonds were detected with Guanine and adenosines Nuclides in one DNA helix but with shorter H-bonds binding to the as seen in Fig. 10b. The interactions are located at DNA DA17: H3—O=C (ligand) with 2.03 Å, DNA DG16:H22—O=C(ligand) with 2.49 Å H-bond and DNA DA18:O4….H-O(ligand) with 1.88 Å (Fig. 10c). The total binding energy was found to be -8.12 Kcal/mol. Therefore, the docking interactions and energy result reflected the ligand as a very good binder. H-bonds positions were consistent with the H-bonds detected in the crystal lattice.

4. Conclusion

The (*Z*)-pyrazol β-keto-enol was proved by the XRD-crystal and the DFT/XRD-structure parameters showed a high matching. Moreover, the H-bonds that were computed via MEP and HSA reflected an excellent matching with the experimental XRD-packing result too. MAC and NPA population charge analysis detected both electrophilic and nucleophilic sites on the molecule surface. The HOMO/LUMO, TD-SCF/DFT, DOS and B3LYP-IR, calculations are in

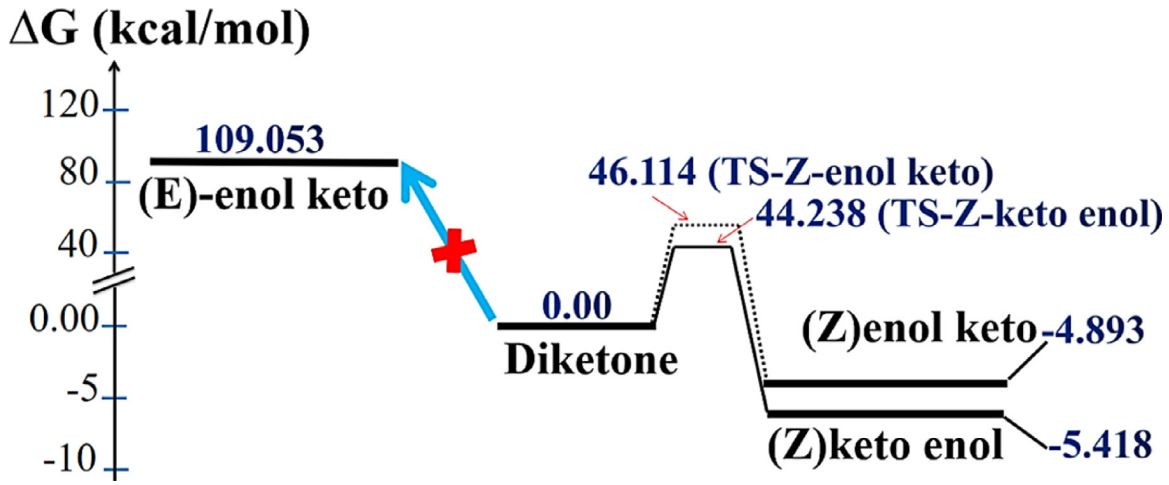

Fig. 8. Gibbs free energy difference profile vs. reaction coordinate for tautomerism structure diketone including implicit SMD solvation [37] of toluene at 273.15 K and 1 atm. All Gibbs free energies are obtained relatively to the Gibbs free energy value of diketone (-3385.694 a.u.); where 1u.a. = 627.509 kcal/mol.

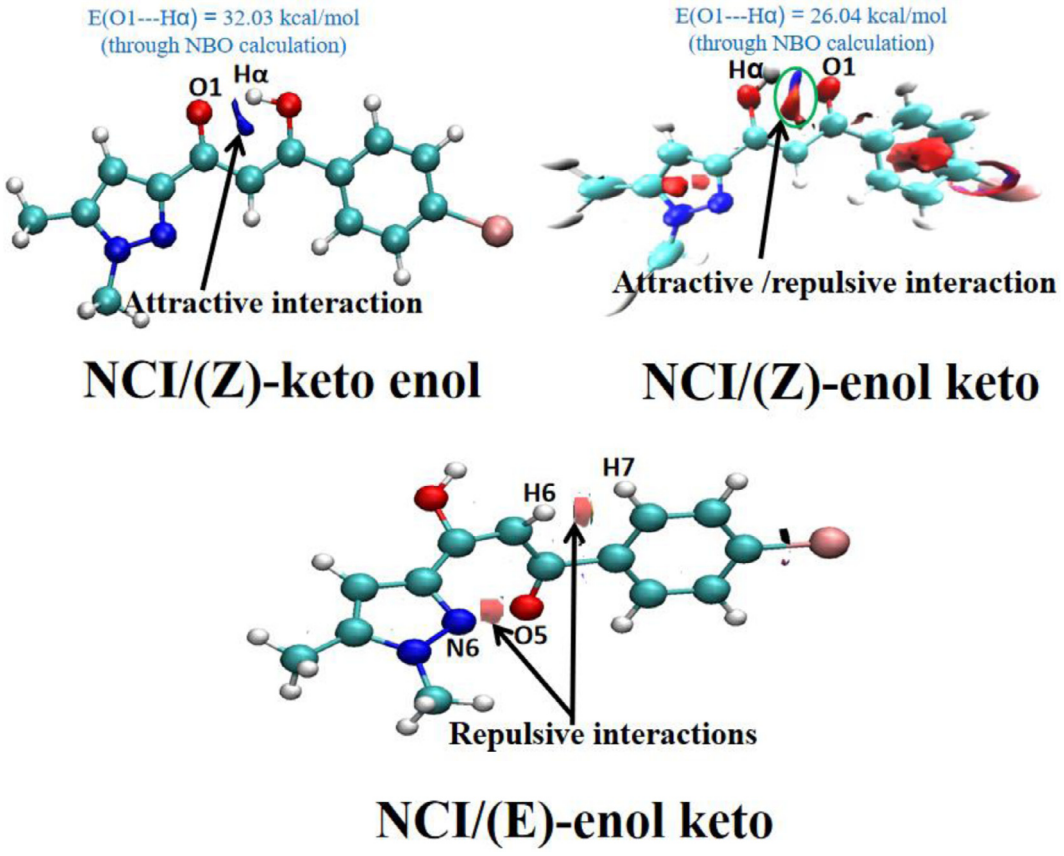

Fig. 9. NCI analysis of (Z)-keto enol, (Z)-enol keto and (E)-enol keto.

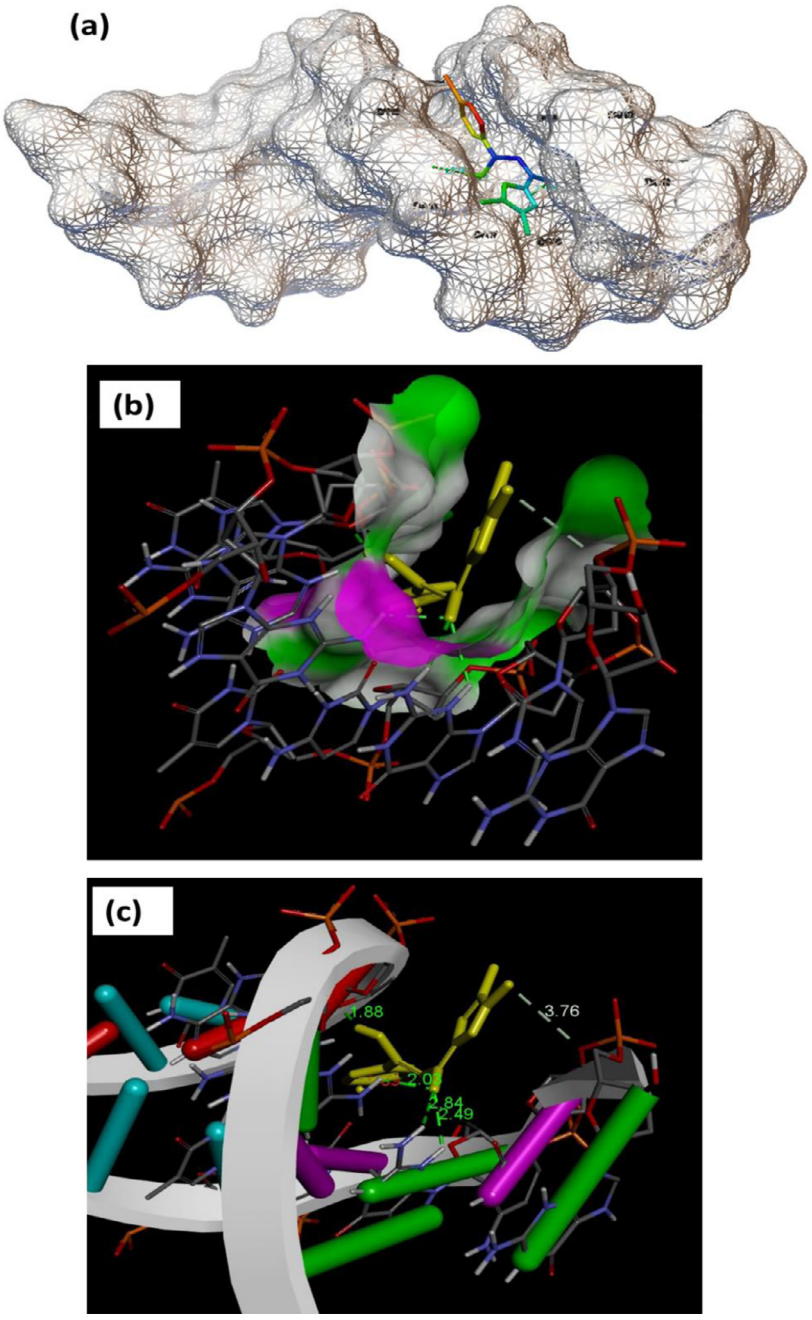

Fig. 10. (a) DNA-ligand binding position representation, (b) tow helix interactions and (c) ligand:Nuclides H-bonds.

an excellent agreement with exp. direct Tauc ΔE_g, UV-visible, FT-IR, spectra. DFT computations and both NBO and NCI analysis. They together indicate clearly that the formation of keto-enol is kinetically more favored than enol-keto; in high approval with experimental data. The results of *in-vitro* antidiabetic activity reflected that the desired molecule exhibited a potent α-glucosidase inhibition with IC_{50} value of 72.20 ± 1.50 µM. The desired compound showed a very good DNA-docking effect and double helix minor grove with four H-bonds binding mode were detected.

Declaration of Competing Interest

The authors declare that they have no conflicts of interest.

CRediT authorship contribution statement

Said Tighadouini: Conceptualization, Validation, Formal analysis, Writing – original draft, Writing – review & editing. **Othmane Roby:** Conceptualization, Validation, Formal analysis, Writing – original draft, Writing – review & editing. **Salma Mortada:** Conceptualization, Validation, Formal analysis, Writing – original draft, Writing – review & editing. **Zouhair Lakbaibi:** Conceptualization, Validation, Formal analysis, Writing – original draft, Writing – review & editing. **Smaail Radi:** Conceptualization, Validation, Formal analysis, Writing – original draft, Writing – review & editing. **Anas Al-Ali:** Conceptualization, Validation, Formal analysis, Writing – original draft, Writing – review & editing. **My El Abbes Faouzi:** Conceptualization, Validation, Formal analysis, Writing – original draft, Writing – review & editing. **Marilena Ferbinteanu:** Conceptualization, Validation, Formal analysis, Writing – original draft, Writing – review & editing. **Yann Garcia:** Conceptualization, Validation, Formal analysis, Writing – original draft, Writing – review & editing. **Nabil Al-Zaqri:** Conceptualization, Validation, Formal analysis, Writing – original draft, Writing – review & editing. **Abdelkader Zarrouk:** Conceptualization, Validation, Formal analysis, Writing – original draft, Writing – review & editing. **Ismail Warad:** Conceptualization, Validation, Formal analysis, Writing – original draft, Writing – review & editing.

Acknowledgements

The authors extend their appreciation to the Researchers Supporting Project number (RSP-2021/396), King Saud University, Riyadh, Saudi Arabia.

Supplementary materials

Supplementary material associated with this article can be found, in the online version, at doi:10.1016/j.molstruc.2021.131308.

References

[1] Y. Goldgur, R. Craigir, GH. Cohen, T. Fujiwara, T. Yoshinaga, T. Fujishita, H. Sugimoto, T. Endo, H. Murai, DR Davies, Structure of the HIV-1 integrase catalytic domain complexed with an inhibitor: a platform for antiviral drug design, Proc. Natl. Acad. Sci 96 (1999) 13040.
[2] A. Minassi, G. Sanchez-Duffhues, JA. Collado, E. Munoz, G. Appendino, Dissecting the pharmacophore of curcumin. Which structural element is critical for which action, J. Nat. Prod. 76 (2013) 1105.
[3] W. Pluymers, G. Pais, BV. Maele, C. Pannecouque, V. Fikkert, R. Burke, E. Clercq, M. Witvrouw, N. Neamati, Z. Debyser, Inhibition of human immunodeficiency virus type 1 integration by diketo derivatives, Antimicrob. Agents. Chemother. 46 (2002) 3292.
[4] K. Adams, J. Cai, J. Armstrong, M. Herold, J. Lu, A. Sun, P. Snyder, D. Liotta, EF24, a novel synthetic curcumin analog, induces apoptosis in cancer cells via a redox-dependent mechanism, Anti-Cancer Drug 16 (2005) 263.
[5] L. Tan, A. Ali, Y. Du, H. Fu, H. Jin, M. Chin, M. Khan, Go L, Synthesis and evaluation of bisbenzylidenedioxotetrahydrothiopranones as activators of endoplasmic reticulum (ER) stress signaling pathways and apoptotic cell death in acute promyelocytic leukemic cells, J. Med. Chem. 57 (2014) 5904.
[6] G. Liang, L. Shao, Y. Wang, C. Zhao, Y. Chu, J. Xiao, Y. Zhao, X. Li, S. Yang, Exploration and synthesis of curcumin analogues with improved structural stability both in vitro and in vivo as cytotoxic agents, Bioorg. Med. Chem. 17 (2009) 2623.
[7] P. Anand, G. Thomas, AB. Kunnumakkara, C. Sundaram, KB. Harikumar, B. Sung, St. Tharakan, K. Misra, K. Priyadarsini IK, N. Rajasekharan, Biological activities of curcumin and its analogues (Congeners) made by man and Mother Nature, Biochem. Pharmaco 76 (2008) 1590.
[8] G. Liang, X. Li, L. Chen, S. Yang, X. Wu, E. Studer, E. Gurley, B. Hylemon, F. Ye, Y. Li, Synthesis and anti-inflammatory activities of mono-carbonyl analogues of curcumin, Bioorg. Med. Chem. Lett. 18 (2008) 1525.
[9] Y. Hui, M. Shu, M. Hu, J. Song, L. Yao, L. Yang, Q. Wu, M. Yang, L. Xue, Syntheses, structures and magnetic properties of tetranuclear and trinuclear nickel (II) complexes with β-diketone-functionalized pyridinecarboxylate ligand, Inorg. Chim. Acta 363 (2010) 3238.
[10] N. Verma, D. Juneja, Synthesis and Characterization of 1-(2′, 4′ dihydroxy-5-nitrophenyl)-3-(pyridin-3-yl)- propane-1, 3-dione and its metal complexes, J. Chem .Tech. Res. 4 (2012) 1000.
[11] A. Titi, T. Shiga, H. Oshio, R. Touzani, B. Hammouti, M. Mouslim, I. Warad, Synthesis of novel Cl2Co4L6 clusterusing 1-hydroxymethyl-3, 5-dimethylpyrazole (LH) ligand: Crystal structure, spectral, thermal, Hirschfeld surface analysis and catalytic oxidation evaluation, J. Mol. Struc. 1199 (2020) 126995.
[12] A. Titi, I. Warad, S.M. Almutairi, M. Fettouhi, M. Messali, A. Aljuhani, R. Touzani, A. Zarrouk, One-pot liquid microwave-assisted green aqua-synthesis of neutral trans-Cl_2Cu $(NNOH)_2$: XRD/HSA-interactions, antifungal and antibacterial evaluations, Inorg. Chem. Comm. 122 (2020) 108292.
[13] R. Daengngern, R. Salaeh, T. Saelee, K. Kerdpol, N. Kungwan, Excited-state intramolecular proton transfer reactions of 2, 5-bis (2′-benzoxazolyl) hydroquinone and its water cluster exhibiting single and double proton transfer: a TD-DFT dynamics simulation, J. Mol. Liq. 286 (2019) 110889.
[14] K. Zborowski, A. Korenova, M. Uher, M.L. Proniewicz, Quantum chemical studies on tautomeric equilibria in chlorokojic and azidokojic acids, J. Mol. Struct. 683 (2004) 15.
[15] J. Nawrot-Modranka, E. Nawrot, J. Graczyk, In vivo antitumor, in vitro antibacterial activity and alkylating properties of phosphorohydrazine derivatives of coumarin and chromone, Eur. J. Med. Chem. 41 (2006) 1301.
[16] D. Matosiuk, S. Fidecka, L. Antkiewicz-Michaluk, J. Lipkowski, I. Dybala, A.E. Koziol, Synthesis and pharmacological activity of new carbonyl derivatives of 1-aryl-2-iminoimidazolidine: part 2. Synthesis and pharmacological activity of 1, 6-diaryl-5, 7 (1H) dioxo-2, 3-dihydroimidazo [1, 2-a][1, 3, 5] triazines, Eur. J. Med. Chem. 37 (2002) 761.
[17] D. Matosiuk, S. Fidecka, L. Antkiewicz-Michaluk, I. Dybala, A.E. Koziol, Synthesis and pharmacological activity of 1-aryl-5, 6 (1H) dioxo-2, 3-dihydroimidazo [1, 2-a] imidazoles, Eur. J. Med. Chem. 37 (2002) 845.
[18] K. Sztanke, S. Fidecka, E. Kedzierska, Z. Karczmarzyk, K. Pihlaja, D. Matosiuk, Antinociceptive activity of new imidazolidine carbonyl derivatives.: Part 4. Synthesis and pharmacological activity of 8-aryl-3, 4-dioxo-2H, 8H-6, 7-dihydroimidazo [2, 1-c][1, 2, 4] triazines, Eur. J. Med. Chem. 40 (2005) 127.
[19] C. Temperini, A. Cecchi, A. Scozzafava, C.T. Supuran, Carbonic anhydrase inhibitors. Comparison of chlorthalidone and indapamide X-ray crystal structures in adducts with isozyme II: when three water molecules and the keto– enol tautomerism make the difference, J. Med. Chem. 52 (2009) 322.
[20] M. Frisch, G. Trucks, H. Schlegel, G. Scuseria, M. Robb, J. Cheeseman, G. Scalmani, V. Barone, B. Mennucci, G. Petersson, in: Gaussian 09 Revision A, Gaussian Inc., Wallingford CT, 2009.
[21] S. K. Wolff, D. J. Grimwood, J. J. McKinnon, D. Jayatilaka, and M. A. Spackman, Crystal explorer 2.1. University of Western Australia, Perth (2007).
[22] G.M. Sheldrick, A short history of SHELX, ActaCryst. 64 (2008) 112.
[23] O. Trott, A. Olson, Auto Dock Vina, J. Comp. Chem. 31 (2010) 455.
[24] Available for free in protein data bank as PDB file at https://www.rcsb.org/structure/1BNA
[25] A. Benallou, Z. Lakbaibi, H. Garmes, H. EL Alaoui, EL Abdallaoui, The role of the polarity on the mechanism and selectivity in the [3+ 2] cycloaddition reaction between CF3-ynone ylide and azide group: a quantum chemical investigation, J. Fluorine. Chem. 219 (2019) 79.
[26] Z. Lakbaibi, H. Abou El Makarim, M. Tabyaoui, A. El Hajbi, Theoretical study of the formation of α-bromoglycidic esters in aliphatic series using the DFT quantum mechanical method with B3LYP/6-311G (d,p), Mor. J. Chem. 4 (2016) 437.
[27] A. Barakat, M. Islam, A. Al-Majid, H.A. Ghabbour, S. Atef, A. Zarrouk, I. Warad, Quantum chemical insight into the molecular structure of l-chemosensor 1, 3-dimethyl-5-(thien-2-ylmethylene)-pyrimidine-2, 4, 6-(1 H, 3 H, 5 H)-trione: naked-eye colorimetric detection of copper (II) anions, J. Theor. Comput. Chem. 17 (2018) 1.
[28] A. Barakat, S.M. Soliman, H.A. Ghabbour, M. Ali, A.M. Al-Majid, A. Zarrouk, I. Warad, Intermolecular interactions in crystal structure, Hirshfeld surface, characterization, DFT and thermal analysis of 5-((5-bromo-1H-indol-3-yl) methylene)-1, 3-dimethylpyrimidine-2, 4, 6 (1H, 3H, 5H)-trione indole, J. Mol. Struct. 1137 (2017) 354.
[29] I. Warad, F.F. Awwadi, B. Abd Al-Ghani, A Sawafta, N. Shivalingegowda, N.K. Lokanath, M.S. Mubarak, T. Ben Hadda, A. Zarrouk, F. Al-Rimawi, A.B. Odeh, S.A. Barghouthi, Ultrasound-assisted synthesis of two novel [$CuBr(diamine)_2 \bullet H_2O$] Br complexes: Solvatochromism, crystal structure, physicochemical, Hirshfeld surface thermal, DNA/binding, antitumor and antibacterial activities, Ultrasonics Sonochem 48 (2018) 1.

[30] I. Warad, S. Musameh, A. Sawafta, P. Brandão, C.J. Tavares, A. Zarrouk, S. Amereih, A. Al Ali, R. Shariah, Ultrasonic synthesis of Oct. trans-$Br_2Cu(N\cap N)_2$ Jahn-Teller distortion complex: XRD-properties, solvatochromism, thermal, kinetic and DNA-binding evaluations, Ultrasonics Sonochem 52 (2019) 428.
[31] M.R. Aouad, M. Messali, Nadjet Rezki, Nabil Al-Zaqri, I. Warad, Single proton intramigration in novel 4-phenyl-3-((4-phenyl-1H-1, 2, 3-triazol-1-yl) methyl)-1H-1, 2, 4-triazole-5 (4H)-thione: XRD-crystal interactions, physicochemical, thermal, Hirshfeld surface, DFT realization of thiol/thione tautomerism, J. Mol. Liq. 264 (2018) 621.
[32] I. Warad, H. Suboh, N. Al-Zaqri, A. Alsalme, F.A. Alharthi, M.M. Aljohani, A. Zarrouk, Synthesis and physicochemical, DFT, thermal and DNA-binding analysis of a new pentadentate N 3 S 2 Schiff base ligand and its [CuN 3 S 2] 2+ complexes, RSC Adv 10 (2020) 21806.
[33] J. Tauc, A. Menth, States in the gap, J. Non-Cryst. Solids 8 (1972) 569.
[34] A. Benallou, Z. Lakbaibi, H. Garmes, H.E.A. El Abdallaoui, The role of the polarity on the mechanism and selectivity in the [3+ 2] cycloaddition reaction between CF3-ynone ylide and azide group: a quantum chemical investigation, J. Fluo. Chem. 219 (2019) 79.
[35] Z. Lakbaibi, H. Abou El makarim, M. Tabyaoui, A.EL Hajbi, Study of the solvent effects on the formation of α-bromoglycidic esters in aliphatic series using the quantum DFT method with B3LYP/6-311G (d,p), J. Mater. Environ. Sci. 8 (2016) 99.
[36] A. Jaafar, H.Ben El Ayouchia, Z. Lakbaibi, A. Boussaoud, S. Jodeh, K. Azzaoui, M. Tabyaoui, Degradation of Pollutant Dye in Aqueous Solution using Fenton Reaction: A DFT Study, Res. J. Chem. 3 (2019) 53.
[37] K. Jana, B. Ganguly, DFT Study To Explore the Importance of Ring Size and Effect of Solvents on the Keto–Enol Tautomerization Process of α-and β-Cyclodiones, ACS Omega 3 (2018) 8429.
[38] R. Chaudret, B.D. Courcy, J. Contreras-García, E. Gloaguen, A. Zehnacker-Rentier, M. Mons, J.P. Piquemal, Unraveling non-covalent interactions within flexible biomolecules: from electron density topology to gas phase spectroscopy, Phys. Chem. Chem. Phys. 16 (2014) 9876.
[39] T. Lu, W F., Chen, Multiwfn: a multifunctional wavefunction analyzer, J. Comput. Chem. 33 (2012) 580.
[40] W. Humphrey, A. Dalke, K. Schulten, VMD: visual molecular dynamics, J. Mol. Graphics 14 (1996) 33.
[41] V. Bertolasi, V. Ferretti, P. Gilli, X. Yao, C-J. Li, Substituent effects on keto–enol tautomerization of β-diketones from X-ray structural data and DFT calculations, New J. Chem. 32 (2008) 694.